Research Article

Insights of Herbal Medicine

The refractive index and dispersion of the sensors are dependent on the parameters of the photonic crystal fibers

Mohammed Salim Jasim*

Gifted Guardianship Committee, Missan Directorate of Education, Misan, Iraq.

***Corresponding author**
Mohammed Salim Jasim, Gifted Guardianship Committee, Missan Directorate of Education, Misan, Iraq.

Submitted: 10 Oct 2022; **Accepted:** 17 Oct 2022; **Published:** 31 Oct 2022

Citation: *Jasim, m. s. (2022). The refractive index and dispersion of the sensors are dependent on the parameters of the photonic crystal fibers. Insights Herbal Med, 1(1), 40-44.*

Abstract

A refractive index sensor based on photonic crystal fibers (PCFs) using finite element method (FEM) has been suggested in this paper. The designed fiber has a hexagonal cladding structure running around its solid core, with six air holes rings. Using the FEM, effective refractive index, confinement loss, fundamental mode laser profile, and sensor resolution are investigated. This constructed sensor characterized by low confinement loss and high resolution such that a small change in the analyte refractive index could be detected which could be useful in detecting changes in biological molecule reaction information as well as in medical applications in areas such as toxins, medication residues, vitamins, antibodies, proteins and parasites.

Key words: Photonic Crystal Fibers(PCFs), Finite Element Method (FEM), Refractive Index Sensor (RIS).

Introduction

Sensors of photonic crystal fibers (FCFs), which in recent decades have attracted particular attention due to their specific advantages of flexibility, high sensitivity, compact size, low cost and fast response, have been widely used in many fields of sensing applications [1-3]. PCFs sensor typically obtains the measurement of strain , temperature, curvature and other quantities by calculating the change in intensity or wavelength shift. Most of these optical sensors are calculating the variations in optical properties due to a transition in the PCF refractive index (RI) [4]. Measuring the RI of PCFs is very important in order to illustrate the optical properties of PCFs that lead to the development of RI sensors for use in many fields, biotechnology processes also play an important role in the interaction of drug / DNA and cell growth [2,5,6].

A new form of optical fiber was developed, named Photonic Crystal Fibers (PCFs), in which air holes along the fiber structure were developed [7]. PCFs may be categorized by guidance mechanism, the core is solid in this form, and the cladding is represented by two-dimensional air holes lattices running around the entire length of the fiber. The RI of the index-guiding PCFs is higher than the cladding, so that the light inside the fiber core is guided through total internal reflection, whereas in the band-gap type, the light is guided by a two-dimensional photonic band-gab, since the core of these fibers is air or (hollow core) less than the refractive index of the cladding. Because of the band-giving phenomena, specific light frequencies that propagate along the fiber are not allowed to escape from the core, but are reflected and constructively interfered within the core and destructively interfered in the core it, Figure (1) shows two types of PCFs [8,9].

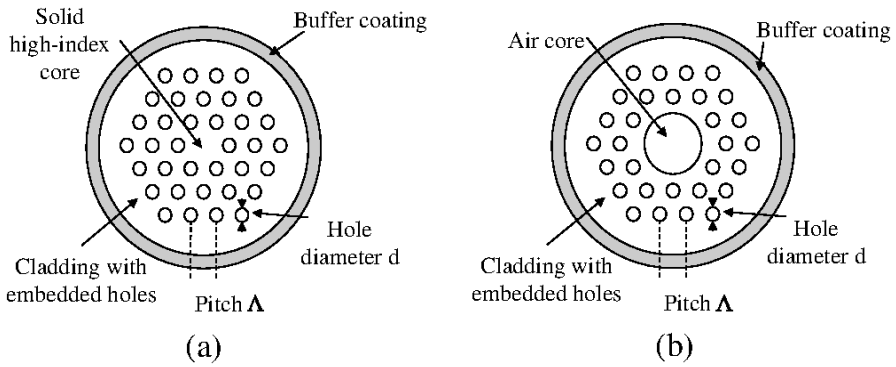

Figure 1: shown PCF microstructure cladding (a) solid core and (b) hollow core PCF [10].

PCFs are designed very flexibly. Manipulating lattice pitch, air hole shape and diameter, refractive glass index, and type of lattice are several parameters. Several techniques can be used to compensate with the wavelength for the dispersion and the area effect, one of which changes the diameter of the air-hole lattice [11-12]. Pulse dispersion is one of the two most significant factors restricting the efficiency of a fiber (the other is the loss of fiber) [13]. Pulse dispersion occurs for four principal reasons [14]:
1.Intermodal Dispersion.
2. Material Dispersion.
3. Waveguide Dispersion.
4. Polarization Mode Dispersion (PMD)

An electromagnetic wave, such as the light emitted by an optical fiber, is essentially a mixture of electrical and magnetic fields that oscillate perpendicularly. When an electromagnetic wave travels over free space.

The dispersion equation depends on the wave- length D (λ) gives by the relation [15-17]

$$D(\lambda) = (-\ {}^{2\pi\, C}/_{\lambda^2}\ )\beta_2\ = ({}^{\lambda}/_{c})(\ {}^{d^2 n_{eff}(\lambda)}/_{d\lambda^2}\ )$$

Unit for (D) is (*ps*/(*nm.km*) and (n_{eff}) the effect refraction factor for both core and cladding of PCFs by the relation [18]:

$$n_{eff}(\lambda) = n_{air}\frac{\left({}^{d}/_{\Lambda}\right)N}{0.5\ {}^{d}/_{\Lambda}} + n_{silica}\,(\lambda)\frac{\left(1-{}^{d}/_{\Lambda}\right)N + 0.5\ {}^{d}/_{\Lambda}}{\left(0.5\ {}^{d}/_{\Lambda}\right)+N}$$

Where (n_{air}) air refractive index, n_{silica} (λ) the effective refractive index for silica material and which compute from the equation

$$n_{eff} = n\,(\lambda\,) = \sqrt{1 + \frac{A\lambda^2}{\lambda^2 - D} + \frac{B\lambda^2}{\lambda^2 - E} + \frac{C\lambda^2}{\lambda^2 - F}}$$

Where, A,B,C,D,E,F, is Sellmeier factor, are constants depend on the material, and experimental compute [19-21]for pure silica (sio_2) the values are:
A= 0.069675, B=0.408218, C= 0.890815, D=0.0047701, E= 0.0133777, F= 98.02107, and (λ) is the wavelength measure by (microns) [22].

Solution Method

To know how to propagate the electromagnetic wave, it is necessary to use Finite Difference Frequency- Domain (FDFD), within the methods of finite-difference, to target the solution of Maxwell's equations by means of a frequency-domain approach, alternatively. This was described for the first time by Zhu et al., for photonic crystal fibers, and we will shortly outline the basic elements of this method. Zhu et al., have used two discretization schemes in the Finite-Difference Frequency-Domain (FDFD) mode solvers [23]. One is that first proposed by Stem, in which there are possible discontinuities between two adjacent mesh grids and each grid point corresponds to a unique refractive indices [24]. The wave equation for the transverse electrical field E_t (or magnetic field H_t) can be expressed as follows:

$$(\nabla_t^2 + k_\circ^2\varepsilon_r)E_t + \nabla(\varepsilon_r^{-1}\nabla_r .E_t) = \beta^2 E_t \ldots \quad (1)$$

$$\nabla_t^2 + k_\circ^2\varepsilon_r)\,H_t + \nabla(\varepsilon_r^{-1}\nabla_r .H_t) = \beta^2 H_t \ \ldots \quad (2)$$

Where $k_\circ = 2\pi/\lambda$ is the wave number in free space,ε_r is the waveguide dielectric constant, and β is the propagation constant . These equations are directly discretized by finite difference as presented in [25]. Typically, the transverse magnetic components are used to derive the discretization matrix [26,27]. In the study by Zhu et al., a full-vector finite-difference mode solver that is based on discretization scheme first proposed by Yee is presented. Yee's mesh, which is widely used in the FDTD analysis [23,28,29]. Zhu et al. use Yee's two-dimensional mesh for complex optical waveguides in their frequency-domain mode solver. Before looking more closely at this method, it should be noted, however, that an index averaging technique is used for cells across interfaces in order to improve the stair approximation for the curved interface [23]. In Yee's mesh, grids for electrical fields are based on possible dielectric discontinuities. Since all the transverse field components are tangential to the unit cell boundary, the continuity conditions are automatically satisfied. Zhu et al., [23] assumes that the fields are dependent on the position z and the time t according to exp[j (-βz+wt)]. From Maxwell's curl equations

$$\nabla \times E = -\frac{\partial B}{\partial t}, \qquad \nabla \times H = \frac{\partial D}{\partial t}$$

After scaling E by the free- space

$$jk_{\circ}H_x = -\frac{\partial E_z}{\partial y} + j\beta E_y \ldots \quad (3)$$

$$jk_{\circ}H_y = j\beta E_x + \frac{\partial E_z}{\partial x} \ldots \quad (4)$$

$$jk_{\circ}H_z = -\frac{\partial E_y}{\partial x} + \frac{\partial E_x}{\partial y} \ldots \quad (5)$$

And

$$jk_{\circ}\varepsilon_r E_x = \frac{\partial H_z}{\partial y} + j\beta H_y \ldots \quad (6)$$

$$jk_{\circ}\varepsilon_r E_y = -j\beta H_x - \frac{\partial H_z}{\partial x} \ldots \quad (7)$$

$$jk_{\circ}\varepsilon_r E_z = \frac{\partial H_y}{\partial x} - \frac{\partial H_x}{\partial y} \ldots \quad (8)$$

Equation (3-8) are now discretized, and Zhu etal., Obtains the following type of equations:

$$jk_{\circ}H_x(i,j) = -\frac{[E_z(i,j+1) - E_z(i,j)]}{\Delta y + j\beta E_y(i,j)} \ldots \quad (9)$$

$$jk_{\circ}H_y(i,j) = j\beta E_x(i,j) + \frac{[E_z(i+1,j) - E_z(i,j)]}{\Delta x} \ldots \quad (10)$$

$$jk_{\circ}H_z(i,j) = -\frac{[E_y(i+1,j) - E_y(i,j)]}{\Delta x + [E_x(i,j+1) - E_x(i,j)]/\Delta y} \ldots \quad (11)$$

The equations (6-8) can be composed in a similar way. Note that the terms j in the brackets indicate a number (and this number has nothing to do with the complex term that appears outside the brackets). Note, moreover, that Zhu et al., approximate the refractive indices by averaging the refractive indices of adjacent cells. Eqs (6-8) may be written in the form of a matrix as follows:

$$-jk_{\circ}\begin{bmatrix} H_x \\ H_y \\ H_z \end{bmatrix} = \begin{bmatrix} 0 & j\beta I & U_y \\ -j\beta I & 0 & -U_x \\ -U_y & U_x & 0 \end{bmatrix}\begin{bmatrix} E_x \\ E_y \\ E_z \end{bmatrix} \ldots \quad (12)$$

$$-jk_{\circ}\begin{bmatrix} \varepsilon_{rx} & 0 & 0 \\ 0 & \varepsilon_{ry} & 0 \\ 0 & 0 & \varepsilon_{rz} \end{bmatrix}\begin{bmatrix} E_x \\ E_y \\ E_z \end{bmatrix} = \begin{bmatrix} 0 & j\beta I & V_y \\ -j\beta I & 0 & -V_x \\ -V_y & V_x & 0 \end{bmatrix}\begin{bmatrix} H_x \\ H_y \\ H_z \end{bmatrix} \ldots \quad (13)$$

where I is a square identity matrix, and ε_{rx} ,ε_{ry} ,and ε_{rz} are diagonal matrices determined by the following equations:

$$\varepsilon_{rx}(i,j) = [\varepsilon_r(i,j) + \varepsilon_r(i,j+1)]/2 \ldots \quad (14)$$

$$\varepsilon_{ry}(i,j) = [\varepsilon_r(i,j) + \varepsilon_r(i-1,j)]/2 \ldots \quad (15)$$

$$\varepsilon_{rz}(i,j) = \begin{bmatrix} \varepsilon_r(i,j) + \varepsilon_r(i-1.j-1) + \\ \varepsilon_r(i,j-1) + \varepsilon_r(i-1,j) \end{bmatrix}/4 \ldots \quad (16)$$

In Eqns. (12-13), the matrices U_x ,U_y,V_x, and V_y, are square matrices, which depend on the boundary conditions of the rectangular computation window.For more details on how these are represented, please consult[23].

Now that a set of matrix equations including the finite difference formulation have been developed, these can be solved using available numerical routines of eigenvalue, which then provide the effective modal index $A_{eff} = \beta/k_{\circ}$ and the guided modes modal fields. The approximation of the staircase has to be used in the rectangular mesh in the finite differential analysis of waveguides with curved interfaces. To improve that approximation, Zhu, et,. al. Use average refractive indices over the interface for mesh cells. In the plane-wave expansion method and in the FDTD analysis, similar techniques have been used before. Using the interfacial cell average refractive index can significantly accelerate convergence and improve the accuracy of modeling for waveguides with curved interfaces, such as PCF.

The diameter of air holes influence on the effective refractive index and dispersion

To know the diameter air hole effect of the photonic crystal fiber by dispersion curve for Gaussian pulse, will be change the diameter air hole as a from d=[(0.5,0.8,1,1.2,1.4)μm] with binding other value such as number of hole (N),wavelength, and pitch value equal 2.8μm .will be acquisition the follows show in figures below:

(a)

(b)

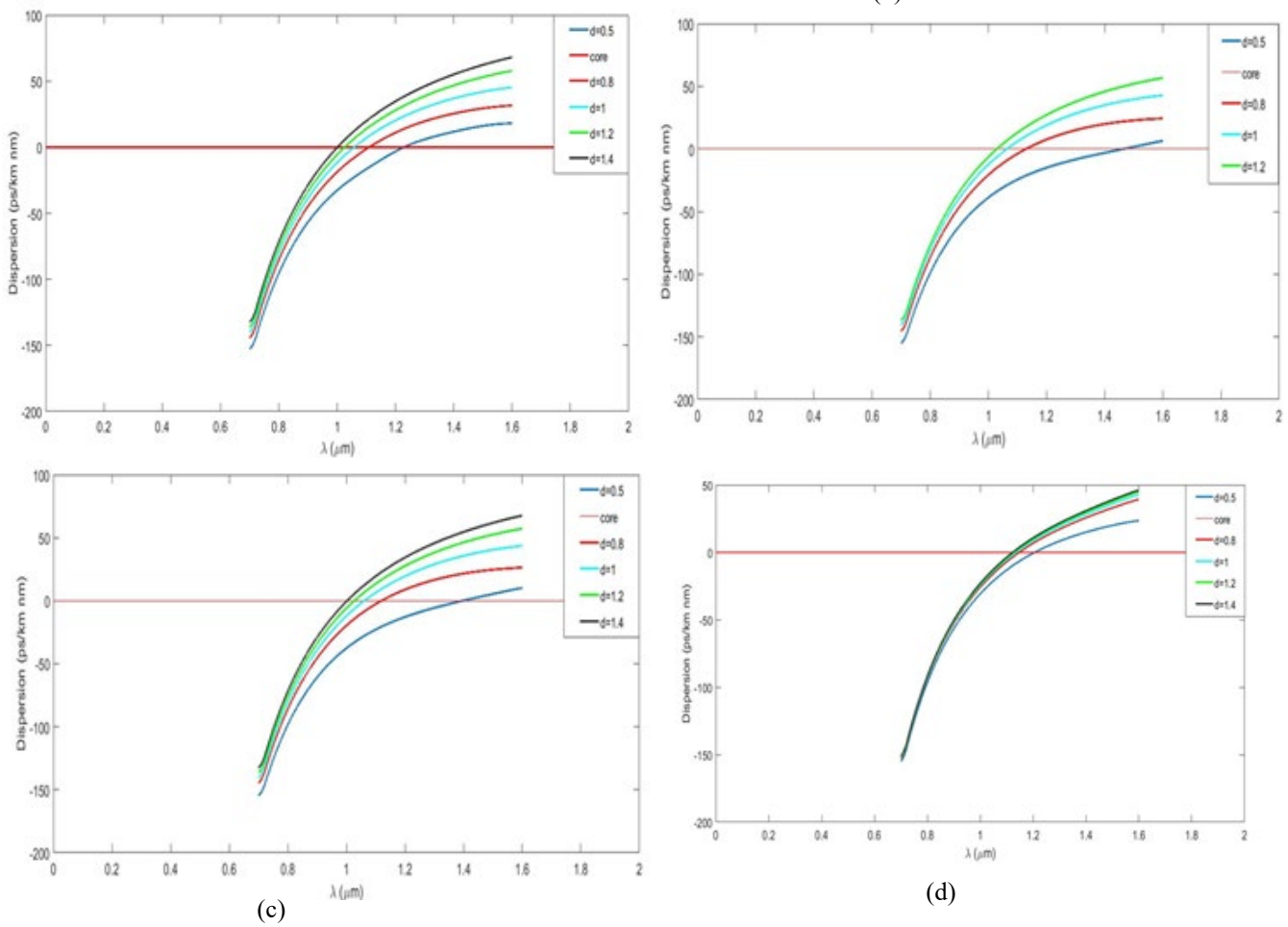

(c)

(d)

Figure 2: for dispersion curves with different values of diameter air hole when (a) N=8, (b) N=10, (c) N=12, (d) N=14. and pitch =2.8

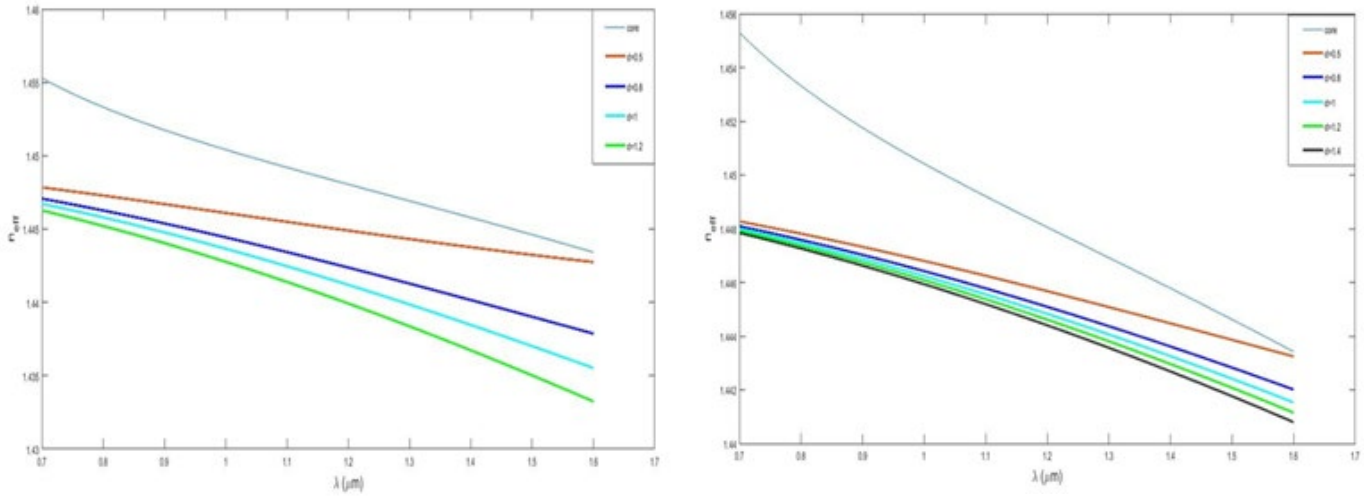

(a)

(b)

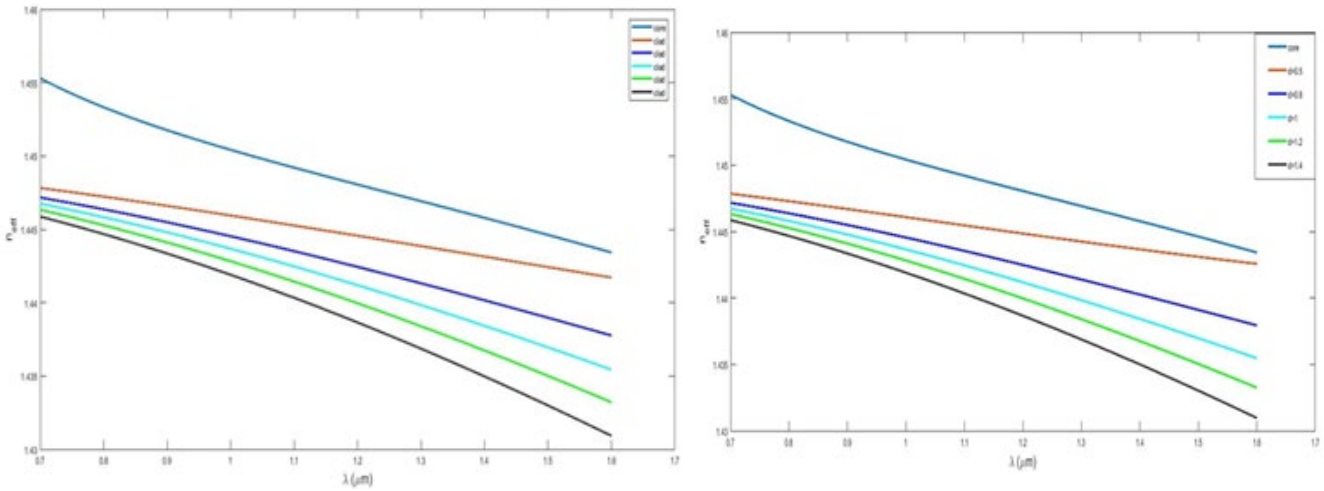

(c) (d)

Figure 3: for effect reflective index curves with different values of diameter air hole when (a) N=8,(b) N=10,(c) N=12,(d) N=14. and pitch =2.8

Result and Discussion

In this study, fixing the value for N and Λ , with different value of d which equal d=0.5,0.8,1,1,1.2,1.4.The relation between dispersion curve for photonic crystal fiber,and pulse wavelength for above value,when the number of hole rings (N=8), as show in figures (a),observed whenever the air hole diameter increased, the zero dispersion (ZD) shifting toward short wave length, whereas dispersion value increased with increase of d value too, that mean we can be control of the zero dispersion for PCFs, by air hole diameter controlled.

When increase the value of N will be obtain the same consequences above-mentioned, show in figures (d),.increase N for(N=12) notice whenever d increase via (d=0.5-1.2),the ZD shifting eastward toward long wavelength and convergence the curves as show in figure (d).Number of ring increase (N=10) for the same value of (pitch, wavelength) with different value of d, we obtain the same consequence above-mentioned,as show in figures (b,c), when (N=12,14), notice the curves of cladding refracted index are convergence both, with increase value of d, also, decreasing of refracted index value at large value of d, over and above notice decrease the different between the core refracted index and cladding refracted index when d increased.

Conclusion

Successfully developed a PCFs sensor based on parameters of resonance to detect refractive index and dispersion. Numerical analyzes based on finite element method were used to investigate both the sensor's structure and performance. The set of conditions perfectly suited the air hole diameter, the number of air holes and the pitch, features to absorb the energy emitted from the device. Optimizing structural parameters to increase sensitivities. Of all samples, the effective refractive index has been reduced by raising the wavelength range, and the fundamental modes are also highly confined in the core region of air-infiltrated samples whose RI is lower than the silica RI, the light is propagated by total internal reflection. Due to its high resolution and low confinement loss, this PCF RI-sensor may be used in various medical and environmental sensing applications using specific d, N, and ubiquitous analytes.

References

1. Leung, C. K., Wan, K. T., Inaudi, D., Bao, X., Habel, W., Zhou, Z., ... & Imai, M. (2015). Optical fiber sensors for civil engineering applications. Materials and Structures, 48(4), 871-906.
2. Wang, X., Lou, S., Sheng, X., & Liang, S. (2016). Simultaneous measurement of torsion, strain and temperature using a side-leakage photonic crystal fiber loop mirror. Infrared Physics & Technology, 76, 603-607.
3. De, M., Gangopadhyay, T. K., & Singh, V. K. (2019). Prospects of photonic crystal fiber as physical sensor: An overview. Sensors, 19(3), 464.
4. Mohebbi, M. (2015). Refractive index sensing of gases based on a one-dimensional photonic crystal nanocavity. Journal of Sensors and Sensor Systems, 4(1), 209-215.
5. Portosi, V., Laneve, D., Falconi, M. C., & Prudenzano, F. (2019). Advances on photonic crystal fiber sensors and applications. Sensors, 19(8), 1892.
6. Silva, S., Roriz, P., & Frazão, O. (2014, December). Refractive index measurement of liquids based on microstructured optical fibers. In Photonics (Vol. 1, No. 4, pp. 516-529). MDPI.
7. Birks, T. A., Knight, J. C., & Russell, P. S. J. (1997). Endlessly single-mode photonic crystal fiber. Optics letters, 22(13), 961-963.
8. Pristinski, D., & Du, H. (2006). Solid-core photonic crystal fiber as a Raman spectroscopy platform with a silica core as an internal reference. Optics letters, 31(22), 3246-3248.
9. Benabid, F., Knight, J. C., Antonopoulos, G., & Russell, P. S. J. (2002). Stimulated Raman scattering in hydrogen-filled hollow-core photonic crystal fiber. Science, 298(5592), 399-402.
10. Yeh, P., Yariv, A., & Marom, E. (1978). Theory of Bragg fiber. JOSA, 68(9), 1196-1201.
11. Osório, J. (2017). “Specialty optical fibers for sensing”

PhD thesis, XLIM Research Institute, USA.
12. Ferrando, A., Silvestre, E., Miret, J. J., Monsoriu, J. A., Andrés, M. V., & Russell, P. S. J. (1999). Designing a photonic crystal fibre with flattened chromatic dispersion. Electronics letters, 35(4), 325-327.
13. Birks, T. A., Knight, J. C., & Russell, P. S. J. (1997). Endlessly single-mode photonic crystal fiber. Optics letters, 22(13), 961-963.
14. Diba, D. D. (2010). PHOTONIC BANDGAP FIBERS. Umea University, Department of Physics, Advanced Materials 7.5 ECTS.
15. Hasan, M., Ahmed, S. N., & Mohiuddin, M. (2011). Study of soliton propagation inside optical fiber for ultra-short pulse (Doctoral dissertation, BRAC University).
16. Vukovic, N. (2010). Optical properties of long photonic crystal fibre tapers (Doctoral dissertation, University of Southampton).
17. Akhmediev, N., Soto-Crespo, J. M., Vouzas, P., Devine, N., & Chang, W. (2018). Dissipative solitons with extreme spikes in the normal and anomalous dispersion regimes. Philosophical Transactions of the Royal Society A: Mathematical, Physical and Engineering Sciences, 376(2124), 20180023.
18. Chen, D., Tse, M. L. V., & Tam, H. Y. (2010). Optical properties of photonic crystal fibers with a fiber core of arrays of subwavelength circular air holes: Birefringence and dispersion. Progress In Electromagnetics Research, 105, 193-212.
19. Shreitah, I., Haji, B. K. (2013)." High Nonlinear photonic crystal fiber (PCF) design with very low confinement loss", Tishreen University J. for Res. and Sci. studies- Eng.Sci. series, Vol.35.
20. Yuan, W. (2013). 2–10 μm mid-infrared supercontinuum generation in As2Se3 photonic crystal fiber. Laser Physics Letters, 10(9), 095107.
21. Liu, S., & Li, S. G. (2013). Numerical analysis of photonic crystal fiber with chalcogenide core tellurite cladding composite microstructure. Chinese Physics B, 22(7), 074206.
22. A.Bjarklev, J.Broeng and A.S.Bjarklev,"photonic crystal fiber",1st Edition, Springer,Denmark,(2003).
23. Zhu, Z., & Brown, T. G. (2002). Full-vectorial finite-difference analysis of microstructured optical fibers. Optics express, 10(17), 853-864.
24. Stern, M. S. (1988). Semivectorial polarised finite difference method for optical waveguides with arbitrary index profiles. IEE Proceedings J (Optoelectronics), 135(1), 56-63.
25. Huang, W. P., & Xu, C. L. (1993). Simulation of three-dimensional optical waveguides by a full-vector beam propagation method. IEEE journal of quantum electronics, 29(10), 2639-2649.
26. Dong, H., Chronopoulos, A., Zou, J., & Gopinath, A. (1993). Vectorial integrated finite-difference analysis of dielectric waveguides. Journal of lightwave technology, 11(10), 1559-1564.
27. Lusse, P., Stuwe, P., Schule, J., & Unger, H. G. (1994). Analysis of vectorial mode fields in optical waveguides by a new finite difference method. Journal of Lightwave Technology, 12(3), 487-494.
28. Yee, K. (1966). Numerical solution of initial boundary value problems involving Maxwell's equations in isotropic media. IEEE Transactions on antennas and propagation, 14(3), 302-307.
29. Kunz, K. S., & Luebbers, R. J. (1993). The finite difference time domain method for electromagnetics. CRC press.